C_{60}-dyad aggregates: Self-organized structures in aqueous solutions

O. A. Guskova, S. R. Varanasi, and J.-U. Sommer

Citation: The Journal of Chemical Physics **141**, 144303 (2014); doi: 10.1063/1.4896559
View online: https://doi.org/10.1063/1.4896559
View Table of Contents: http://aip.scitation.org/toc/jcp/141/14
Published by the American Institute of Physics

C_{60}-dyad aggregates: Self-organized structures in aqueous solutions

O. A. Guskova,[1,a)] S. R. Varanasi,[1,a),b)] and J.-U. Sommer[1,2]
[1]*Leibniz-Institut für Polymerforschung Dresden e.V., Hohe Straße 6, Dresden D-01069, Germany*
[2]*Institut für Theoretische Physik, Technische Universität Dresden, Zellescher Weg 17, Dresden D-01069, Germany*

(Received 23 July 2014; accepted 2 September 2014; published online 8 October 2014)

Extensive full-atomistic molecular dynamics simulations are performed to study the self-organization of C_{60}-fullerene dyad molecules in water, namely phenyl-C_{61}-butyric acid methyl ester and fulleropyrrolidines, which have two elements of ordering, the hydrophobic fullerene cage and the hydrophilic/ionic group. While pristine fullerene or phenyl-C_{61}-butyric acid methyl ester forms spherical droplets in order to minimize the surface tension, the amphiphilic nature of charged solute molecules leads to the formation of supramolecular assemblies having cylindrical shape driven by charge repulsion between the ionic groups located on the surface of the aggregates. We show that formation of non-spherical micelles is the geometrical consequence if the fullerene derivatives are considered as surfactants where the ionized groups are only hydrophilic unit. The agglomeration behavior of fullerenes is evaluated by determining sizes of the clusters, solvent accessible surface areas, and shape parameters. By changing the size of the counterions from chloride over iodide to perchlorate we find a thickening of the cylinder-like structures which can be explained by stronger condensation of larger ions and thus partial screening of the charge repulsion on the cluster surface. The reason for the size dependence of counterion condensation is the formation of a stronger hydration shell in case of small ions which in turn are repelled from the fullerene aggregates. Simulations are also in good agreement with the experimentally observed morphologies of decorated C_{60}-nanoparticles. © *2014 AIP Publishing LLC*. [http://dx.doi.org/10.1063/1.4896559]

I. INTRODUCTION

Spheres, vesicles, needles, rods, tubules, disks, stars, and fibers of nanometer dimensions were obtained as a result of ordered association of fullerene derivatives, which was promoted by solvent variations. The solubility of fullerenes, which up to some extent could be an important factor of aggregate geometry,[1,2] includes two essential aspects. First of all, these are specific molecular interactions between the fullerene and solvent molecules, i.e., intermolecular forces. Apart from the effect of size and nature of the forces, the solubility and/or the formation of one particular spatial aggregate shape over another is governed by molecular geometrical features: the molecular size (because C_{60} is a sub-colloidal particle with diameter ∼1 nm) and the fullerene geometry – the molecular surface area and the molecular volume.

Usually the interaction between solute and solvents causes the conformational changes of the dissolved molecules. The pristine fullerenes with their unique cage structure have a rigid and well defined shape, which is not changing upon dissolution.[3] The old rule "like dissolves like" can describe a high solubility of fullerene C_{60} in aromatic hydrocarbons and their derivatives, whose structure is close to that of the regular hexagons inherent on the C_{60} surface.[4,5] But even in non-polar, good solvents, fullerenes can readily form self-assembled molecular clusters, whose size and shape can be altered with structural modifications of C_{60}-cage or by changing the solvation process.[6]

In polar solvents, including water, the fullerenes are virtually insoluble and tend to form colloidal systems with nanoscale dimensions (d = 25–500 nm),[7–9] also known as "nano-C_{60}."[10] The extremely high hydrophobicity of fullerene, coupled with a tendency to form aggregates, hampers its direct biomedical application.[11] Moreover, *in vitro* toxicity of fullerenes is correlated with its ability to undergo aggregation, because the fullerene clusters may effectively bind with biomacromolecules and deactivate them or alter their functions.[12,13] In addition, precise control over the aggregate geometry via the compatibility tuning is a rational strategy for tailoring bicontinuous electron donor and fullerene-based acceptor arrays for the solution-processable optoelectronic thin films.[14] Furthermore, very recently fullerene derivatives have been proposed as a new buffer layer for inverted polymer/fullerene solar cells with improved power conversion efficiency.[15]

There have been several attempts to overcome the natural repulsion of fullerenes from water and to control their aggregative behaviour.[16] This problem has been solved to a great extent by various supramolecular (1)–(3) and chemical (4) approaches to functionalizing fullerenes:

(1) the solubilisation of fullerenes using different solubility enhancers – surfactant micelles,[17] liposomes,[18] and lipid membranes,[19,20] which are of biopharmaceutical interest for covering biocompatible surfaces or for the controlled release of drugs;

a)Authors to whom correspondence should be addressed. Electronic addresses: guskova@ipfdd.de and s.raovaranasi@uq.edu.au
b)Present address: School of Chemical Engineering, University of Queensland, St Lucia 4072, Australia.

(2) complexes with water-soluble biomacromolecules[21] and synthetic polymers;[22,23]
(3) receptor-ligand (C_{60}) complexes;[24,25]
(4) chemical functionalization to increase the hydrophilicity, for instance with amino acids, carboxylic acids, polyhydroxyl groups, amphiphilic polymers, etc. [26–35] This way to functionalize the fullerene via attaching a wide range of well-hydrated groups to the carbon core has led to improved solubility in polar media. The hydrophilic décor has also become a critical element to promote and modulate supramolecular aggregation and to shift a paradigm from the self-assembly to commanded assembly of smart fullerene-based materials.[36]

Hydrophilically modified fullerenes can be considered as unusual surfactants, because in contrast to the conventional tenside molecules, they combine a polar tail and a hydrophobic head. According to the presently available data, short hydrophilic groups attached to a fullerene core benefit the formation of spherical aggregates, while long ionic groups favour linear (rod-like, cylinder-like) aggregates. Such water-soluble C_{60}-carrying single-chain ammonium amphiphiles are also known as artificial fullerene lipids due to their ability to form bilayers.[37] The impact of geometrical characteristics of the building C_{60}-units on the final shape and morphology of the nanostructures resembles the aggregative behaviour of phospholipids, that is controlled by head group size, molecular volume, and solvent-exposed areas.[38] This simple but very efficient approach for the prediction of packing ability of surfactant molecules in water from the curvature of the water-lipid interface is based on the concept of critical packing parameter (CPP), which is expressed as the ratio between the volume of the hydrophobic tail, v, and the product of the cross-sectional lipid head area, A, and the lipid chain length, l.[39] For typical surfactant systems in mostly aqueous media CPP $<$ 1/3 for spherical micelles, ranges from 1/3 to 1/2 for cylindrical micelles, from 1/2 to 1 for flexible bilayers or vesicles, equals 1 for planar bilayers, and greater 1 for inverted micelles. Of course, the ratios of volumes and surface areas of the hydrophilic/hydrophobic counterparts of fullerene derivatives are remarkably different even from those of double-chained phospholipids having small head groups and therefore inverted cone geometry.

This concept has been applied for the packing behaviour prediction of fullerene dyads on different substrates and in the bulk.[40,41] In fact, considering the C_{60} group as the head moiety instead of the hydrophilic part in surfactants has led to the discrepancy between theoretically predicted and experimentally observed structures.[42] This is due to the fact that the aggregative behaviour of fullerenes is a multifaceted problem, as mentioned above, and apart from the purely geometrical features includes also the aspect of intermolecular interactions. First of all, the C_{60} head group is not a hydrophilic component and causes a strong π–π interaction, which is not equivalent to the hydrophilic interactions of surfactants in aqueous media.[40] On the other hand, the tendency of substituents, e.g., alkyl tails, to crystallize/form an interdigitated conformation in assemblies of the derivatives, the effects of solvents, surface effects,[41] electrostatic interactions including the type of counterion,[42,43] etc. may shift the observed structures from micelles to the planar bilayers and inverted phases. Therefore a more advanced theoretical description based on computer simulation techniques is needed to rationalize the shape of fullerene dyad aggregates including the analysis of intermolecular interactions and the packing motifs.

Addressing some of these fundamental questions, Mortuza and Banerjee[44] have theoretically studied the agglomeration of PCBM (phenyl-C_{61}-butyric acid methyl ester) in various organic solvents and their mixtures. Extensive molecular dynamics simulations revealed the correlation between agglomeration behaviour of nanoparticles and processing temperature, solute concentration, and solvent type. The role of intermolecular donor/acceptor, π-π, and van der Waals interactions between fullerene acceptor and electron-rich *N*,*N*-dimethylaminoazobenzene addend has been investigated within a joint experimental-theoretical approach by Kumar and Patnaik.[45] Several groups have reported about structural properties of small highly hydroxylated fullerene clusters, also named fullerol or fullerenol, in aqueous solutions.[46,47] Finally, in a series of papers published by Patnaik *et al.*[5,48,49] the aggregative behaviour of C_{60}-didodecyloxybenzene dyad was studied by a combination of experimental and simulation techniques. The special emphasis was placed on the mechanism of agglomerate growth in binary solvent mixtures, which goes through several stages of the self-assembly.[50]

In the present article, motivated by experimental observations,[51,52] we discuss the results of full-atomistic molecular dynamic simulation of amphiphilic-C_{60} derivatives in water. The main scope is to provide insight into the molecular interaction types responsible for the dyad aggregate self-assembly. The focus is on phenomena that determine the shape of the final ensemble in water.

This paper is organized as following. Section II describes the simulation framework – the model and the methods – used to imitate the organic molecules dispersed in aqueous medium. In Sec. III the molecular aggregation is discussed as a multifaceted phenomenon, which is driven by the competition between several intermolecular forces. The last part summarizes the results as well as discusses the overall themes, which pertain to self-organization motifs of the fullerene dyads. Finally, it concludes with suggestions for future experiments and computer simulations, which should fill in the remaining gaps in the present understanding of hydrophilic fullerene-based materials.

II. COMPUTATIONAL MODEL AND METHODS

In this paper the term “dyad” is used to underline two elements of ordering, the hydrophobic fullerene cage and the hydrophilic (ionic) group. The dyad molecules are phenyl-C_{61}-butyric acid methyl ester (PCBM although is not strictly an amphiphile, the presence of hydrophilic ester group makes the molecule polar) and ionic fullerene derivatives, fulleropyrrolidines,[52] which chemical formulas are depicted in Fig. 1. Monosubstituted fulleropyrrolidines have the solubilizing addend in *N*-position, which ends with terminal ammonium group (quaternary ammonium cation). The counterions are chloride, iodide, or perchlorate. Their

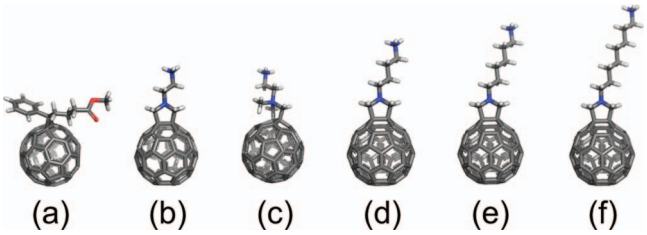

FIG. 1. Optimized structures of fullerene dyads: (a) PCBM, (b), (d)–(f) fulleropyrrolidines cations, and (c) fulleropyrrolidine dication. Grey, red, white, and blue sticks represent carbon, oxygen, hydrogen, and nitrogen atoms, respectively; PyMOL visualization.[53]

number is always equal to the number of organic cations (Figs. 1(b) and 1(d)–1(f)) or doubled in the case of quaternary ammonium dication (Fig. 1(c)). The difference between fulleropyrrolidines (b)–(f) is the addend chain length (for fulleropyrrolidines the "attached" organic moieties are 2-pyrrolidin-1-ylethylammonium (b), 2-(1-methyl-pyrrolidin-1-yl)-ethylammonium (c), 4-pyrrolidin-1-ylbutylammonium (d), 6-pyrrolidin-1-ylhexylammonium (e) and 8-pyrrolidin-1-yloctylammonium (f), Fig. 1). Fully optimized molecular geometries (Fig. 1) are found by using density functional theory with hybrid B3LYP functional and 6-31G(d) basis set implemented in Gaussian 09 software.[54]

In our MD simulations, we employed the polymer consistent force field[55] supplemented by some additional parameters related to fullerene nanoparticle. For C_{60}, the parameters for Lennard-Jones (LJ) potential are taken from the work of Girifalco ($\epsilon = 0.2763$ kJ/mol, $\sigma = 3.469$ Å).[56] The recent simulations have shown a very good performance of the Girifalco's model for the investigation of fullerene behaviour in aqueous and organic solvents.[57] For terminal ammonium group of the fulleropyrrolidines, the LJ parameters are borrowed from the OPLS-AA force field.[58] The total potential energy of the system is represented as a sum of the bond stretching, bond angle bending, and dihedral torsion energies as well as the van der Waals (LJ) and electrostatic (Coulomb) terms. Both short-range van der Waals and long-range electrostatic interactions between all atoms are explicitly included in the model. LJ parameters for the cross interactions are obtained using the Lorentz-Berthelot mixing rules.

The water molecules are modelled with modified TIP3P potential[59] and O—H bonds (k_b = 1882.8 kJ/mol, b_0 = 0.9572 Å) and H—O—H angles (k_θ = 230.12 kJ/mol, θ_0 = 104.52°) are treated with harmonic potentials. In some calculations the solvent is simulated implicitly, i.e., as continuum medium with dielectric constant of water. The electrostatic interactions are calculated using Ewald summation method.

To obtain a many-molecule system, 32 fullerene dyads (with the same or doubled number of counterions, if needed) in optimized geometry are placed in a cubic box and then solvated with $n = 5000$ or 10 000 water molecules, which are uniformly and randomly distributed over the simulation box. To avoid both any solute pre-association and hydrogen bond contacts between water molecules, the initial cubic simulation box is at least eight times larger, than the volume corresponding to liquid water density (for n water molecules) at $T = 300$ K. All start configurations are generated using PACKMOL software.[60]

At the beginning, all molecular dynamics simulations are carried out in NPT ensemble for 2.5 ns (equilibration time for 500 ps, integration step 1 fs) or until the volume of the system reaches an equilibrium value to obtain the correct density. Starting from this configuration, the simulations are performed in NVT ensemble for 50 ns after an equilibration run of 1 ns. For the case of continuum solvation, the initial configuration contains fullerene derivatives (and counterions), which are randomly arranged in a cubic box of volume corresponding to liquid water density at $T = 300$ K. All simulations are performed at ambient conditions (temperature $T = 300$ K and pressure $P = 1$ atm) using LAMMPS simulation software.[61] Additional details of the simulation procedure can be found in the Ref. 62.

III. RESULTS AND DISCUSSION

A. Critical packing parameter of fullerene dyads

As mentioned above, the actual form assumed by an aggregate depends largely on the molecular constitution of the amphiphile and is explained by geometric considerations.[38,39] Although the predictions made for fullerene amphiphiles are in agreement with a broad range of experimental results,[63,64] this primarily qualitative packing principle still has some limitations.[42] For instance, according to the Tsonchev's study[65] on the packing problem of the amphiphiles having "hard" cone or truncated cone geometry, the spherical aggregate shape is always preferred in the surfactant self-assembly in contrast to the Israelachvili packing rule.[38,39] For example, specially designed fullerene amphiphiles bearing branched or dendritic well-hydrated side groups, whose geometry indeed resembles the truncated cone, behave in line with the model by Tsonchev *et al.* forming small spherical aggregates.[66–68] It should be noted, however, that both approaches focus on the explanation of overall cluster form and not on the local arrangement of the molecules within the cluster. Moreover, as it was outlined in the introduction, there are also other molecular characteristics and experimental factors that should be taken into account to rationalize agglomerate geometries (critical aggregation concentration, thermodynamic, and kinetic factors,[42] non-covalent forces, counterion effect, spacing between the charges and the hydrophobic part[69]).

As mentioned above, to predict what kind of aggregate is to be expected, one needs to know the values of v, A, and l. Nevertheless, *a priori* estimation of the critical packing parameter is a nontrivial task. The major difficulty is related to the evaluation of the effective headgroup area occupied by molecule at the interface which depends on the solute concentration. Furthermore, the theoretical predictions should be considered as qualitative only and need to be confirmed experimentally, but such nanoscopic structural properties are not readily accessible from experiment.[70] There have been some attempts made[42] to estimate the nanoscopic structural properties of fullerene amphiphiles from experiments, but the methods used were indirect and provided a large spread of the values. Finally, there is no universal method to calculate

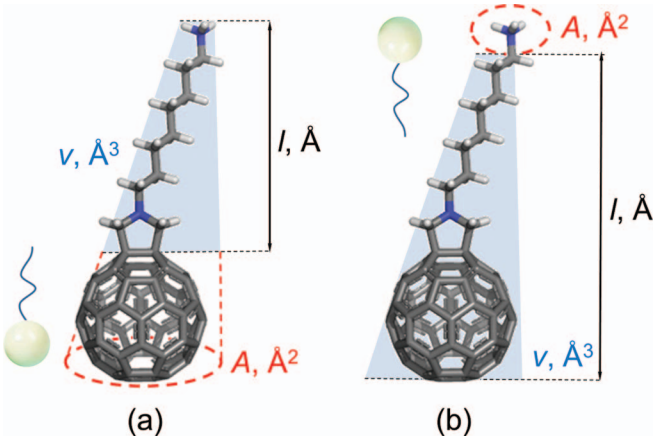

FIG. 2. The definition of dyad molecular dimensions for calculation of the critical packing parameter CPP_1 (a) and CPP_2 (b). Grey, red, white, and blue sticks represent carbon, oxygen, hydrogen, and nitrogen atoms, respectively; PyMOL visualization.[53]

molecular volumes and surface areas. The earliest so called cylindrical model was formulated by Stearn and Eyring.[71] Hard sphere model (or CPK) model was proposed by Corey and Pauling,[72] which is a structure-sensitive alternative to the cylindrical model. However, this approach completely ignores the effect of molecular packing (the void volume). To account for the contribution of the void volume, Lee and Richards defined the surface-accessible surface, which is usually traced by the center of a probe sphere, representing the solvent, rolling over the van der Waals surface of the molecule.[73] Based on electronic properties of the molecules, quantum mechanical models for definition of molecular boundaries by an isodensity surfaces were also proposed, e.g., Bader model,[74] molecular face theory.[75] To the best of our knowledge, only CPK model has been applied for the evaluation of required parameters v, A, and l for the packing prediction of several fullerene dyads.[40,41,50]

Fullerene dyad molecules are not conventional surfactants, unless they resemble them in shape[40] (Fig. 2(a)). On the other hand, C_{60}-"headgroup" is not a hydrophilic one, and the fulleropyrrolidine dyad molecule consists of hydrocarbon "tail" with bulky fullerene cage with a dominant intrinsic geometric constraint and charged ammonium "headgroup" (Fig. 2(b)). Using both the geometrical similarity from one side (Fig. 2(a), CPP_1) and the actual hydrophilic and hydrophobic regions of the molecules from another side (Fig. 2(b), CPP_2), the packing parameters of all fullerene dyads depicted in Fig. 1 are calculated. The definitions of dyad molecular dimensions – the volume of the tail, v, the head area, A, and the "lipid" chain length, l for both approaches are illustrated in Fig. 2.

Because required parameters for given fullerene derivatives v, A, and l cannot be found from experiment, we do not know the real dimensions which molecules have in the micelles. Moreover, the packing parameters are estimated for the molecules in optimized geometries (subject to DFT calculations), i.e., without reference to hydration,[70] conformation or solute concentration. Although this methodology requires some approximations, we believe this approach permits prediction of both the type of self-organizing fullerene structures and the tendency of phase transformations qualitatively, as it was already demonstrated by a series of CPP calculations proposed so far.[5,40,41,48–50] In contrast to the previous studies, the v and A values are estimated using surface accessible surface parameter (probe sphere is water molecule of diameter 1.4 Å). The results are listed in Table I.

TABLE I. Critical packing parameters CPP_1 and CPP_2 calculated for all dyad molecules (Fig. 1).

System	CPP_1	CPP_2
PCBM (a)	0.190	0.530
Fulleropyrrolidine cation (b)	0.130	0.905
Fulleropyrrolidine dication (c)	0.145	0.311
Fulleropyrrolidine cation (d)	0.108	0.746
Fulleropyrrolidine cation (e)	0.102	0.693
Fulleropyrrolidine cation (f)	0.100	0.679

The CPP_1 parameters for all dyad molecules predict the formation of spherical micelles similarly to single-chain lipids with large headgroup areas, because $CPP_1 < 1/3$.[38,39] Taking into account the physical properties of the molecules, i.e., the hydrophilic and hydrophobic regions, CPP_2 values predict different aggregate morphologies. For example, for fulleropyrrolidine dication CPP_2 is equal to 0.311, which corresponds to cylindrical micelle. For fulleropyrrolidine cations, CPP_2 implies the flexible bilayers/vesicles ($CPP = 1/2 \div 1$) or planar bilayers (~ 1).

To relate these parameters to the actual cluster shapes, first it is necessarily to discuss the aggregation process studied in molecular dynamics simulations which are performed for several dyad molecules (PCBM, fulleropyrrolidine mono- and dication (Figs. 1(b) and 1(c)). So, we will return to this discussion later and compare the theory predictions with simulation results and experimentally observed morphologies.

B. Aggregation in aqueous solution

MD simulations of the systems with initially dispersed nanoparticles reveal that fullerene derivatives build aggregates in aqueous solution, which are stable during the simulation time, and no fullerene is present in dissolved state. Figure 3 gives the illustration of clusters formed by PCBM molecules (Fig. 1(a)), fulleropyrrolidine cations with the shortest addend length (Fig. 1(b)) and fulleropyrrolidine dication (Fig. 1(c)). On the basis of visual inspection one can conclude that these aggregates have different shapes: PCBM molecules assemble in almost spherical agglomerate, whereas fulleropyrrolidine cations produce an elongated architecture, which coincides with the prediction of critical packing parameter (Table I, CPP_2). Remarkably, distinct and separate regions composed of the non-polar fullerene parts and the polar parts of the addends, having minimal contact with one another, can be distinguished in the case of charged derivatives (Figs. 3(b) and 3(c)), which means that such elongated micelle has a hydrophobic core and a hydrophilic exterior shell.

To further understand the relative assembling behaviour in the simulated fullerene-water systems, various radial distribution functions (RDFs) are calculated. Figure 4(a)

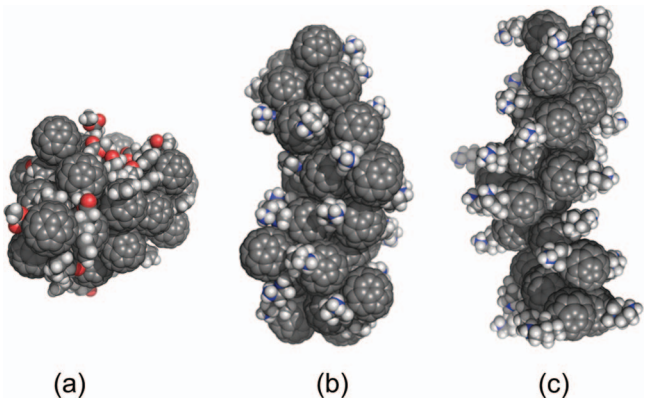

FIG. 3. Snapshots of simulated aggregates of (a) PCBM, (b) fulleropyrrolidine monocation, (c) fulleropyrrolidine dication forming in aqueous solution (explicit model); water molecules (a)–(c) and chloride ions (b) and (c) are omitted for clarity. CPK grey, red, white, and blue spheres represent carbon, oxygen, hydrogen, and nitrogen atoms, respectively; PyMOL visualization.[53]

depicts the fullerene-fullerene radial distribution functions (between fullerene center-of-masses). The RDF curve appears to be more structured with more pronounced peaks in the case of fulleropyrrolidine derivative whereas it is liquid-like for PCBM cluster. In both cases, the first peak appears at around 10 Å which roughly corresponds to the van der Waals diameter of the C_{60} cage. The first peak position is coincident with the location of the minima of the potential of mean force reported by Kim *et al.*[76] This peak is a signature of local coordination due to the formation of agglomerate where the space between the fullerene center-of-masses is the van der Waals cage diameter.[77] But for PCBM, the minimum packing distance is shorter than that of cation-C_{60} derivative. This can be the consequence of reduced hydrophobicity/higher solubility of fulleropyrrolidines in water as compared to non-ionic dyad.

The first peak appears to be broad in the case of PCBM and it is very sharp in the case of the ionic derivative. Also the intensities of the RDF peaks of organic cation suggest that the aggregated structure is non-spherical in shape and also not a three dimensional. Figure 4(b) represents the RDF between nitrogen, hydrogen of terminal ammonium group in the fulleropyrrolidine addend and chloride ion. The terminal nitrogen shows more significant peak at 4 Å and also the terminal hydrogen shows two pronounced peaks at around 4 Å

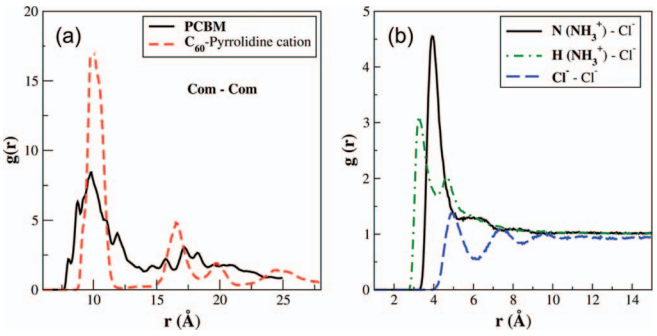

FIG. 4. Radial distribution functions between (a) center-of-masses of solute molecules and (b) nitrogen, hydrogen atoms of the terminal ammonium group of the fulleropyrrolidine monocation and chloride anion and between counterions.

which are separated by a distance of 1 Å. These peaks indicate that there is a close association between nanoparticles and chloride counterions and in particular the counterions stay closer to the terminal ammonium groups where most of the charge on the addend chain is accumulated. The RDF between the Cl^- ions shows a liquid-like structure and the structural features of this function can be seen up to 10 Å, which is also the closest distance of approach of two fullerene moieties. Both charged NH_3 groups and chloride ions are associated with water, the water molecules are preferentially oriented around these species forming several solvation structures.[62]

Because the critical packing parameter (Table I, CPP_1) predicts the formation of spherical micelles for both molecules – PCBM and fulleropyrrolidine with the shortest addend, but in fact for both second and third derivatives the elongated aggregates are observed, the effect of charged groups should be taken into account, namely "the principle of opposing forces," which contributes to the geometry of the resulting structures (Table I, CPP_2).[78,79] There are many types of interaction that are involved in the stabilization of fullerene derivative assemblies. Obvious one is hydrophobic interaction between apolar patches of C_{60}, electrostatic interaction between oppositely and equally charged moieties, hydrogen bonds, structural solvation interaction. For the case of fullerenes, however, the dominant attractive interactions seem to arise from hydrophobic forces acting between hydrocarbon cages. Concerning the repulsion, the pivotal role of surface charge on a typical C_{60} cage has been already demonstrated on the fullerene cluster dissolution in water,[77] where the overall effect of Coulomb interactions has led to the transition from hydrophobic to hydrophilic behaviour.

In very general terms, the behaviour of C_{60}-macroions in polar medium, which represents a thermodynamically poor solvent, resembles the effective attraction of like-charged objects (macroions,[80] polymer brushes,[81] etc.). This type of attraction can universally be observed in ion-containing systems.[82] At more abstract level, this fullerene micelle can be considered as a droplet of a charged liquid in a surrounding solvent, these two liquids being immiscible. The surface tension between these liquids arises from the attraction between fullerene "monomers," which results from the hydrophobicity of the fullerene and promotes the formation of the spherical droplet (pristine C_{60} or PCBM aggregate). But the electrostatic repulsion between charged groups of fullerene monomers (charges on the droplet surface) leads to a shape change of the microscopic droplet (fulleropyrrolidine agglomerate); for larger aggregates Rayleigh instability[82] causes a breakup of a single charged droplet into smaller-sized objects – pearl-necklace structure of the polyelectrolyte chain[80] or bundles of the chains in polyelectrolyte brushes.[81] Thereby, the cluster shape and finite size depends on the balance of opposing forces: the strength of the LJ interaction between monomeric units and the strength of electrostatic interactions, counterion effects, and solvent quality. For the fulleropyrrolidine agglomerates the non-spherical surface generated in water is the result of the action of these opposing forces. "Pro" spherical aggregate formation act strong hydrophobic interactions of C_{60} patches (sphere has a smaller area, i.e., surface energy is released), geometry of the molecules (CPP_1,

Table I) and counterion condensation – the charged colloid agglomerates capture oppositely charged counterions, which form a very thin shell around cluster surface, resulting in a very strong screening affecting the aggregation process. Both surface charge, which tries to break charged spherical clusters or introduce the ellipsoidal deformation of the aggregate, and the interaction between addend chains and solvent molecules work "contra" (spherical) aggregate formation. In addition, the entropic effects due to anisotropic solvation also cannot be ignored because the hydrophobic character of the contact area leads to a significant loss of solvation of the groups involved if removed from the aqueous environment.

To gain quantitative insight into the shape and size of the aggregates formed by different fullerene derivatives, both the calculation of solvent accessible surface area (SASA) and shape analysis are carried out. The solvent accessible surface area is evaluated using VMD visualization program with built-in measure "sasa" command.[83]

In Figure 5, SASA of the agglomerate is shown as a function of time for the whole trajectory for PCBM derivative (a) and (b) and for the ionic C_{60} molecules (b) and (c). The calculated distribution functions of the SASA values for the whole trajectory are shown as an inset of the corresponding plot. In the case of continuum solvation (Fig. 1 of the supplementary material[84] and Figs. 5(b) and 5(d)) the fullerene derivatives aggregate in a similar way that seen in explicit water. Only one single aggregate is formed. However, the size and the shape of the aggregates are different: the aggregates of PCBM cluster are not changing significantly (neither in shape, nor in size) as compared to the explicit solvent simulation, whereas the fulleropyrrolidine micelle demonstrates more spherical shape, as indicates lower mean SASA value (Fig. 5). In the latter case, all counterions are in condensed state, i.e., the Coulomb interactions are screened, and the aggregate shape transforms in the spherical one (Fig. 1 of the supplementary material[84]). Therefore, a transition from anisotropic to continuum (isotropic) solvation causes the condensation of counterions and also does not take into account the anisotropic solvation of solute molecules. Although one can only speculate about the origin of the non-spherical shape of fulleropyrrolidines in aqueous solutions, such simple "experiments" with continuum solvation suggest that long-ranged electrostatics and anisotropic solvation can drive the aggregation of C_{60} dyads in rod-like agglomerates.

Another quantity that is useful for characterizing the shape is so called shape descriptors: asphericity, acylindricity, and relative shape anisotropy.[85] These quantities that examining the aggregate's principal radii of gyration tensors are defined in the reference.[85] At a given time, a radius of gyration tensor for every aggregate is calculated; next, the matrix is diagonalized to find the three eigenvalues, which then are ordered from smallest to largest and averaged. The eigenvectors of the gyration tensor can be interpreted as the geometrical axes of an ellipsoid that effectively approximate the

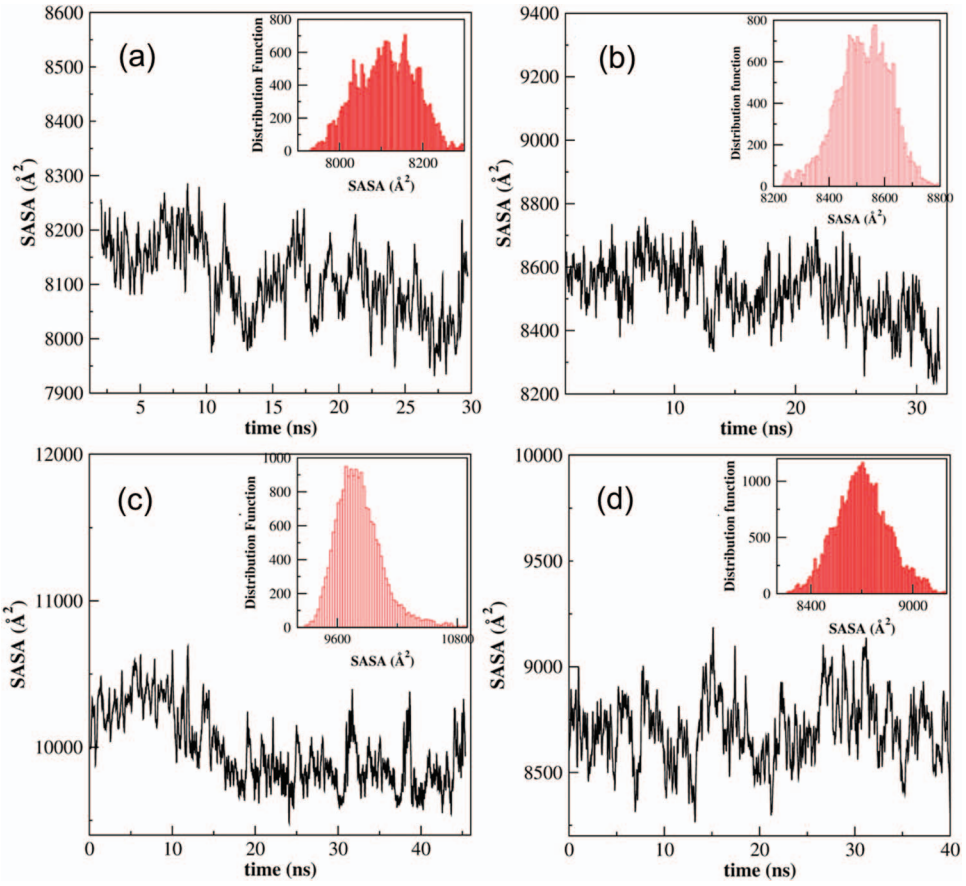

FIG. 5. Time evolution of solvent accessible surface area of the PCBM (a) and (b) and fulleropyrrolidine monocation aggregates (b) and (c) in explicit (a) and (c) and implicit (b) and (d) solvent. The distribution of SASA is shown in the insets of the respective plot.

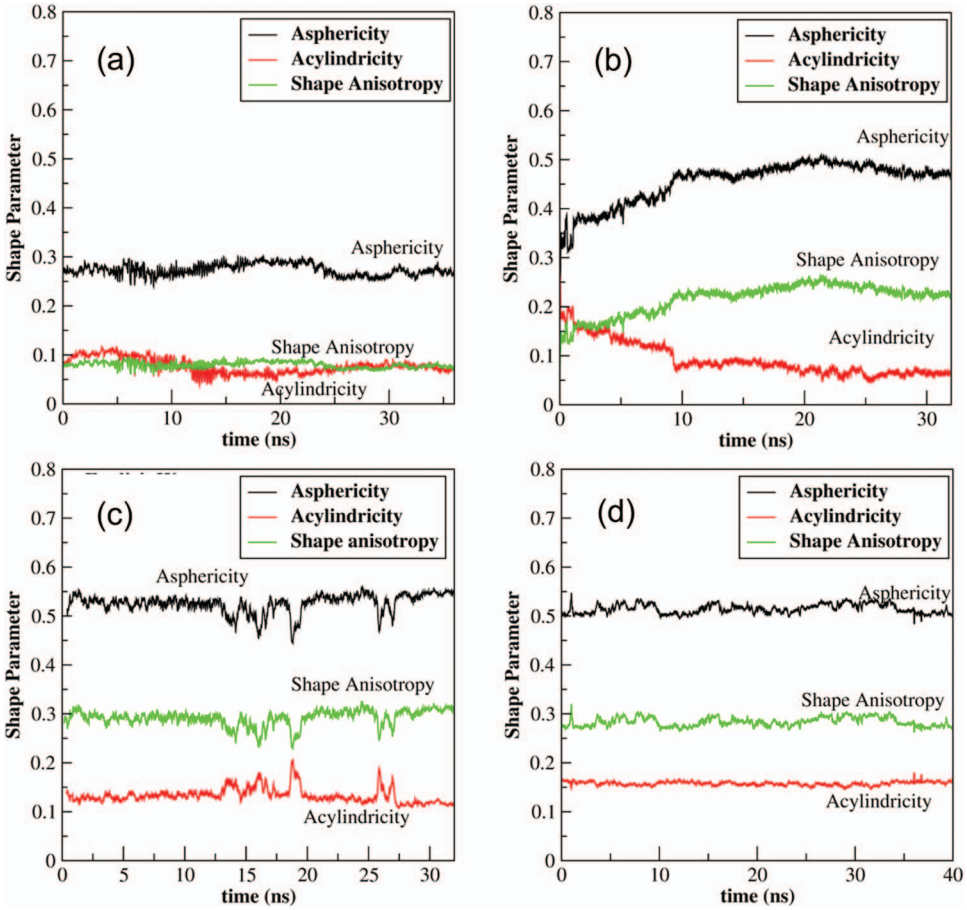

FIG. 6. Time evolution of shape parameters of the PCBM (a) and (b) and fulleropyrrolidine monocation aggregates (c) and (d) in explicit (a) and (c) and implicit (b) and (d) solvent.

average spatial distribution of atoms/molecules with respect to the center of a molecule/cluster. The eigenvalues then correspond to the squares of the length (moments) of the associated elliptic axes.[85] The values of asphericity and acylindricity are equal to zero for the shapes of tetrahedral or higher symmetry and the acylindricity value is equal to zero for the shapes of cylindrical symmetry. The overall shape anisotropy can be calculated from the dimensionless relative shape anisotropy. The relative anisotropy reaches 1 for an ideal linear arrangement and drops to zero in the case of highly symmetric configurations (at least tetrahedral symmetry). For planar symmetric objects, anisotropy converges to the value of 0.25. In Figure 6, the time evolution of all the three shape parameters is collected. The time variation of these shape factors also suggests that the aggregate morphology is stable during the simulation. The asphericity values are fluctuating around 0.5 in all cases except the case of PCBM in explicit water where it fluctuates around 0.3 (average values are given in Table II). PCBM in explicit water seems to have more symmetric morphology as compared to all other

TABLE II. Average solvent accessible surface area probed by water molecule of diameter 1.4 Å and shape descriptors of the clusters in aqueous solution. The averages are calculated for the whole production of the simulated trajectory. The error bars are indicated in the parentheses.

Counterion/solvent model	Surface area (Å^2)	Asphericity	Acylindricity	Shape anisotropy
PCBM				
.../explicit	8141.30(137.90)	0.273(0.011)	0.076(0.016)	0.079(0.007)
.../implicit	8521.11(94.54)	0.453(0.043)	0.092(0.034)	0.217(0.031)
Fulleropyrrolidine monocation				
Chloride/explicit	9980.88(146.77)	0.527(0.019)	0.131(0.014)	0.293(0.016)
Chloride/implicit	8702.88(155.15)	0.519(0.022)	0.156(0.007)	0.289(0.024)
Iodide/explicit	9519.05(176.95)	0.507(0.015)	0.126(0.017)	0.269(0.015)
Perchlorate/explicit	9611.18(191.41)	0.503(0.013)	0.142(0.013)	0.268(0.013)
Fulleropyrrolidine dication				
Chloride/explicit	12 578.6(177.35)	0.410(0.045)	0.154(0.026)	0.217(0.030)

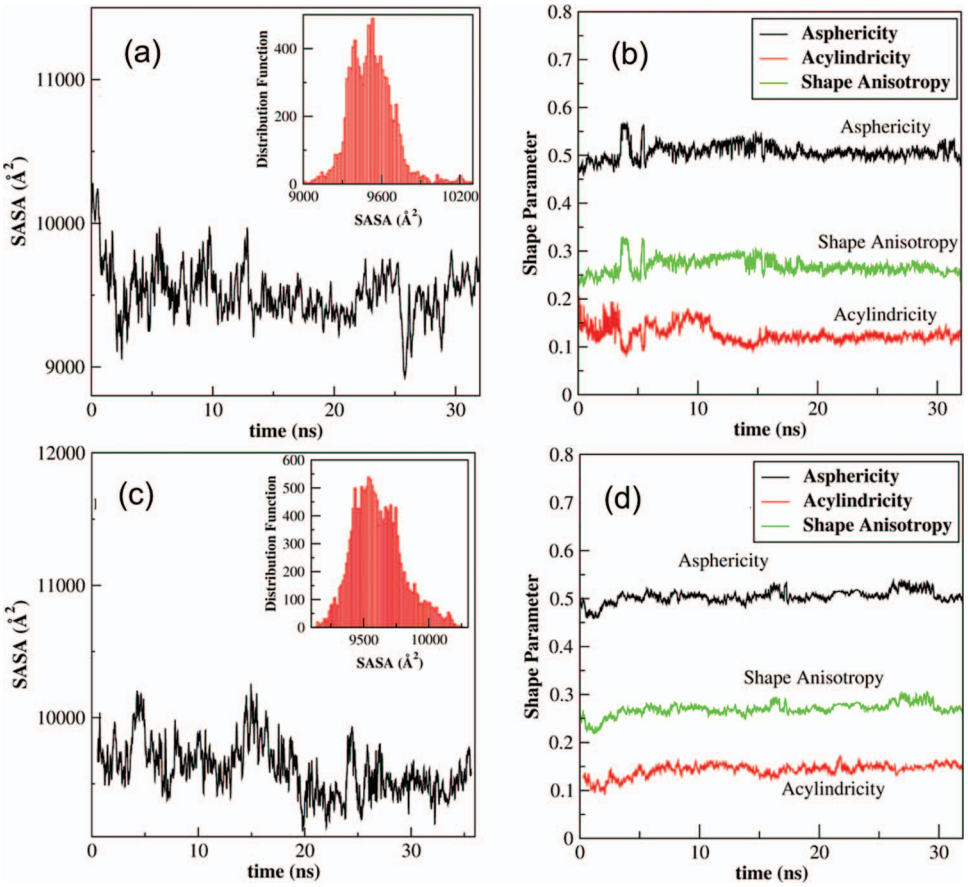

FIG. 7. Time evolution of solvent accessible surface area (a) and (c) and the shape parameters (b) and (d) of the agglomerates of fulleropyrrolidine monocation with iodide (a) and (b) and perchlorate (c) and (d) counterions.

cases. Both lower asphericity and shape anisotropy values for PCBM in explicit water indicate that it is spherical in shape than the aggregate of pyrrolidine-C_{60} cation in explicit water, which shows elongated geometry.

For ion-containing systems – surfactants, synthetic polymers, or protein globules, the fractional charge of the micelle depends upon the counterion, and this in turn influences the size and shape of the micelle,[86] which can be explained in terms of specific ion effects near a surface of sub-colloidal C_{60}-particle/cluster similarly to the Hofmeister interaction.[87] In order to account for the counterion specificity in the formation of cationic fulleropyrrolidine micelles, three anions – chloride, iodide, and perchlorate are selected. In a row $CI^- < I^- < ClO_4^-$ the maximal radius[88] has perchlorate anion, the minimal size – chloride anion, which reflects their hydration behaviour.[89–92] The hydration energy of an anion, as measure of the hydrophilicity/hydrophobicity of the ion, is the free energy for transfer of the unsolvated gas(organic)-phase anion to an aqueous solution. For the CI^--anion, the hydration energy is $\Delta G_h = -340\,\mathrm{kJ\,mol^{-1}}$, for the I^--anion $-275\,\mathrm{kJ\,mol^{-1}}$, and for ClO_4^--anion $-205\,\mathrm{kJmol^{-1}}$.[93] Chloride ion is highly solvated ion with a strong affinity for hydrophilic surfaces and it is known to be depleted from hydrophobic surfaces. On the other hand, the perchlorate anion is poorly solvated inorganic anion, which has very low hydration number and favourable free energy of transfer from water to organic solvents.[94]

In Figure 7, both the time evolution of solvent accessible surface area (a) and (c) and shape factors (b) and (d) for the aggregates of fulleropyrrolidine cation (Fig. 1(b)) in water with chaotropic iodide and perchlorate counterions are plotted (for comparison see also the same aggregate characteristics for kosmotropic chloride anion, Figs. 5(a), 5(c), 6(b), and 6(c) and Table II). The solvent accessible surface area of the aggregate in the presence of larger counterions (iodide and perchlorate) is smaller than for chloride ion. The decrease in surface area indicates the effect of counterion size on the aggregate geometry. In principle, the counterions act by altering one or both of the forces which define the resulting aggregate

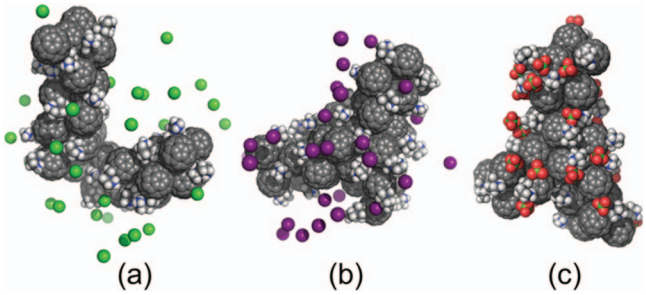

FIG. 8. Snapshots of fulleropyrrolidine monocation aggregates with different counterions in explicit water: (a) chloride anions, green CPK spheres, (b) iodide anion, purple CPK spheres, and (c) perchlorate anions, green-red tetrahedrons; water molecules are omitted for clarity. PyMOL visualization.[53]

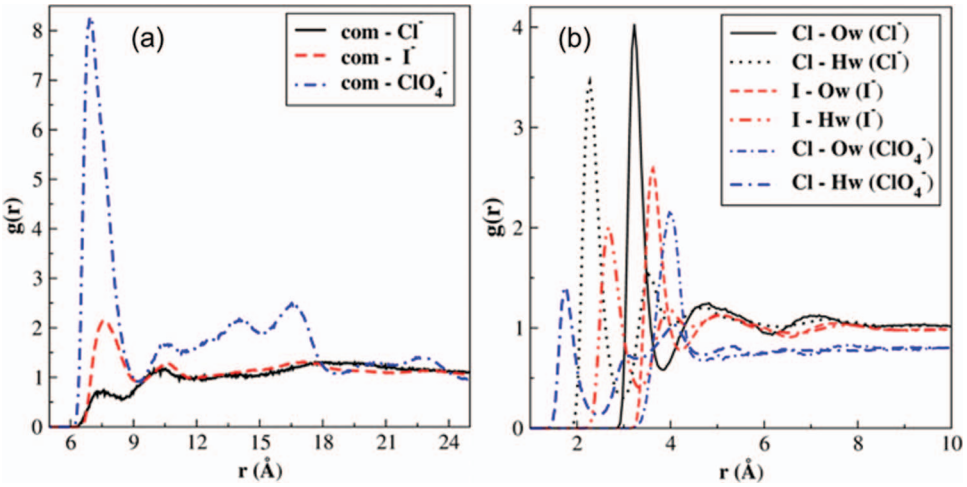

FIG. 9. RDFs between (a) center-of-masses of fulleropyrrolidine monocation and chloride, iodide, perchlorate anions and (b) RDFs between counterions and oxygen, hydrogen atoms of water.

form (Fig. 8): the condensation of counterions onto the micelle surface can reduce repulsive head group interactions and change the interfacial energy at the surface of the micelle.[95]

The mechanism behind this observation, which is tightly bound to the ions hydration behaviour, can be interpreted in terms of ion adsorption at the micellar interface, which depends on the nature of the anions. Adsorption behaviour can be viewed as a partitioning of the anions between the aggregate surface and the bulk solution. Upon examining the distribution functions between these two states (Fig. 9) as well as snapshots from Fig. 8, the following observations can be made. Small, charge-dense ions having large and structured hydration shells do not approach the surface of the solute at short distances; they are repelled from the hydrophobic regions of the fulleropyrollidine molecules (Figs. 8(a) and 9(b)). Large, charge-diffuse anions have thinner hydration shells and display increased affinity to the hydrophobic C_{60} patches of the cluster surface, they behave more like hydrophobic solutes.[90,92] For example, the significant number of perchlorate anions, which reflects in a well-defined maximum of RDF, is present at the cluster surface forming a Stern layer of adsorbed ions. Approaching the cylinder-like surface at closer distances, these anions screen and weaken the electrostatic interactions (Figs. 8(b) and 8(c)) which is also seen from the radial distribution functions (Fig. 9(a)). Such specific counterion condensation of perchlorate (to a smaller extent of iodide) ions inevitably leads to the modification of the aggregate geometry to more spherical in shape, which is similar to pristine C_{60} or PCBM cluster (Figs. 8(c) and 9(a) and Fig. 1 of the supplementary material[84]). The iodide and especially chloride anions are found near the aggregate interface as well as forming a diffuse layer around the cluster. It is interesting to point out that the different behavior of these ions can be attributed to differences in their hydration energies: for the anion to be adsorbed at the aggregate surface, it needs to undergo partial desolvation. The perchlorate anions have relatively low solvation energy mostly because of their generally large size. Therefore, a smaller desolvation penalty is paid compared with the chloride anions.

The shape descriptors of fulleropyrrolidines with larger counterions show small difference from those seen in case of chloride anion. These numbers however support the above mentioned tendency as well – the asphericity, acylindricity, and shape anisotropy values fluctuate around 0.5, 0.15, and 0.25, respectively, i.e., the average structure of fulleropyrrolidine aggregates is still elongated. Thus, the relative effects of

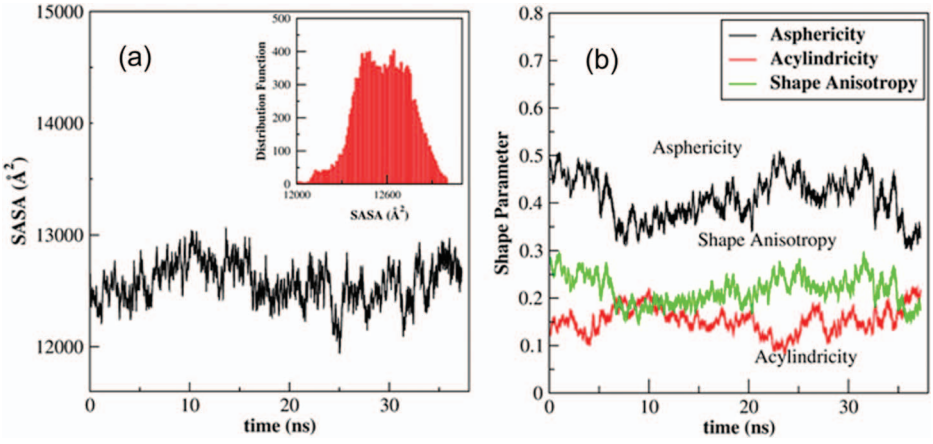

FIG. 10. Time evolution of solvent accessible surface area (a) and the shape parameters (b) of the agglomerates of fulleropyrrolidine dication with chloride counterions.

the anions on the aggregate shape are well explainable by (i) surface effects and (ii) water structure affecting abilities. The latter aspect is clearly seen from the RDFs (Fig. 9(b)).

The simulations of fulleropyrrolidine dication (Figs. 1(c) and 3(c)) with doubled number of chloride counterions reveal the formation of a thin cylinder with the largest SASA surface, as depicted in Table II. In Figure 10, both the time evolution of solvent accessible surface area (a) and shape factors (b) are illustrated. The SASA value is higher (12 578.6 Å^2 vs. 9980.88 Å^2) and the asphericity is lower (0.5 vs. 0.4) as compared to monovalent fulleropyrrolidine cation. Both higher surface area and more elongated shape indicate increased solubility of dicationic C_{60} derivatives due to repulsion of like-charged identical addend chains. Similar mechanism of the fullerene assembling which starts from planar ribbon with C_{60} head-to-head conformation and then transforms into bilayer/vesicle is found to be also electrostatic driven.[50]

IV. CONCLUDING REMARKS

Fullerenes being strongly hydrophobic in nature prefer to build clusters to minimize their nonpolar surface exposed to the polar surroundings depending on both the properties of packing molecules and experimental conditions. The chemical modification of these objects with well-hydrated groups, which provide the solubility in water, offers new routes for controllable molecular self-assembly. In this study, the results of a compromise between the side chain hydrophilicity – the charges on the atoms in the addend chain, that favour contact with water, and the opposing drive of fullerene core was detected for the "model systems" in molecular dynamics simulation. A gentle interplay of acting forces (surface tension/electrostatics) guides molecules of several fullerene dyads to organize themselves into micelles in aqueous solutions. The agglomeration behavior of fullerenes is evaluated by determining sizes of the clusters, solvent accessible surface areas, and shape parameters.

A different type of clustering phenomenon is seen for neutral and charged C_{60}-derivatives. Fullerene with hydrophilic but neutral short ester-side group preferentially forms spherical aggregates in water similarly to pristine C_{60} particles. Fulleropyrrolidines self-assemble in turn into elongated structures because of the presence of charged groups and counterions that help molecules to template themselves into non-spherical structures with hydrophobic core and hydrophilic exterior. By changing the size of the counterions from chloride over iodide to perchlorate we find a thickening of the cylinder structures which can be explained by stronger condensation of larger ions and thus partial screening of the charge repulsion on the cluster surface. The reason for the size dependence of counterion condensation is the formation of a stronger hydration shell in case of small ions which in turn are repelled from the fullerene aggregates. Furthermore, the presence of longer hydrophilic group introduces the more pronounced "linear" stacking (cylindrical micelles, flexible or planar bilayers) which becomes a dominant pathway for fulleropyrrolidine molecules to aggregate.[51,52] Such simple tuning of molecular geometry of fullerene molecules and evaluation of critical packing parameters can be used for elementary empirical estimation of their microstructure. However, the rationalization of the structures only on the basis of amphiphilic packing theories is still need to be realized.

Further simulations will be focused on such factors of self-assembly as the length of the methylene chain of addend, the bis-substitution[96] of the C_{60}-cage representing an extra element of ordering (Fig. 2 of the supplementary material[84]), solvent-based control of agglomerate shape as well as the theoretical investigation of nanoscale amphiphilic polymer/fullerene co-assemblies. The latter case is essential for preparing smart nanostructured materials for the technological applications in the field of organic electronics, because the localization of molecular components (donor and acceptor) having similar polarity in water offers a powerful, nondirectional driving force for the self-assembly and folding of amphiphilic systems.

ACKNOWLEDGMENTS

The authors are very grateful to the Center for Information Services and High Performance Computing (ZIH) of the Technische Universität Dresden for providing CPU time and Dr. Peter Friedel (IPF Dresden) for technical support.

[1]D. M. Guldi, F. Zerbetto, V. Georgakilas, and M. Prato, Acc. Chem. Res. **38**, 38 (2005).
[2]D. M. Guldi and N. Martín, J. Mater. Chem. **12**, 1978 (2002).
[3]R. S. Ruoff, D. S. Tse, R. Malhotra, and D. C. Lorents, J. Phys. Chem. **97**, 3379 (1993).
[4]S. Talukdar, P. Pradhan, and A. Banerjee, Fullerene Sci. Technol. **5**, 547 (1997).
[5]A. Patnaik, Nanosci. Nanotechnol. **7**, 1111 (2007).
[6]L. Liz-Marzan, and P. V. Kamat, in *Nanoscale Materials* (Kluwer Academic, Boston, 2003).
[7]N. O. Mchedlov-Petrossyan, J. Mol. Liq. **161**, 1 (2011).
[8]N. O. Mchedlov-Petrossyan, Chem. Rev. **113**, 5149 (2013).
[9]Y. I. Prylutskyy, A. S. Buchelnikov, D. P. Voronin, V. V. Kostjukov, U. Ritter, J. A. Parkinson, and M. P. Evstigneev, Phys. Chem. Chem. Phys. **15**, 9351 (2013).
[10]J. D. Fortner, D. Y. Lyon, C. M. Sayes, A. M. Boyd, J. C. Falkner, E. M. Hotze, L. B. Alemany, Y. J. Tao, W. Guo, K. D. Ausman, V. L. Colvin, and J. B. Hughes, Environ. Sci. Technol. **39**, 4307 (2005).
[11]B. Manashi, H. Moriyama, and F. Shahidi, in *Bio-Nanotechnology: A Revolution in Food, Biomedical and Health Sciences* (John Wiley & Sons, 2012).
[12]G. Oberdörster, E. Oberdörster, and J. Oberdörster, J. Environ. Health Perspect. **113**, 823 (2005).
[13]S. Radic, P. Nedumpully-Govindan, R. Chem, E. Salonen, J. M. Brown, P. C. Ke, and F. Ding, Nanoscale **6**, 8340 (2014).
[14]K. Sivula, Z. T. Ball, N. Watanabe, and J. M. J. Fréchet, Adv. Mater. **18**, 206 (2006).
[15]N. Wang, L. Sun, X. Zhang, X. Bao, W. Zheng, and R. Yang, RSC Adv. **4**, 25886 (2014).
[16]R. Bakry, R. M. Vallant, M. Najam-ul-Haq, M. Rainer, Z. Szabo, C. W. Huck, and G. K. Bonn, Int. J. Nanomed. **2**, 639 (2007).
[17]M. Dallavalle, M. Leonzio, M. Calvaresi, and F. Zerbetto, Chem. Phys. Chem. **15**, 2998 (2014).
[18]Z. Zhou, Pharmaceutics **5**, 525 (2013).
[19]J. Wong-Ekkabut, S. Baoukina, W. Triampo, I.-M. Tang, D. P. Thileman, and L. Monticelli, Nat. Nanotechnol. **3**, 363 (2008).
[20]J. Barnoud, G. Rossi, and L. Monticelli, Phys. Rev. Lett. **112**, 068102 (2014).
[21]V. I. Bhoi, S. Kumar, and C. N. Murthy, Carbohydr. Res. **359**, 120 (2012).
[22]H. Sawada, J.-I. Iidzuka, T. Maekawa, R. Takahashi, T. Kawase, K. Oharu, H. Nakagawa, and K. J. Ohira, Colloid Int. Sci. **263**, 1 (2003).
[23]S.-I. Yusa, S. Awa, M. Ito, T. Kawase, T. Takada, K. Nakashima, D. Liu, S. Yamago, and Y. Morishima, J. Polym. Sci., Part A: Polym. Chem. **49**, 2761 (2011).

[24]R. M. Williams and J. W. Verhoeven, Recl. Trav. Chim. Pays-Bas **111**, 531 (1992).
[25]G. M. Dell'Anna, R. Annunziata, M. Benaglia, G. Celentano, F. Cozzi, O. Francesconi, and S. Roelens, Org. Biomol. Chem. **7**, 3871 (2009).
[26]U. S. Jeng, T. L. Lin, T. S. Chang, H. Y. Lee, C. H. Hsu, Y. W. Hsieh, T. Canteenwala, and L. Y. Chiang, Prog. Colloid Polym. Sci. **118**, 232 (2001).
[27]P. Zhang, Z. X. Guo, and S. Lv, Chin. Chem. Lett. **19**, 1039 (2008).
[28]N. F. Goldshleger, A. F. Shestakov, E. V. Ovsyannikova, and N. M. Alpatova, Russ. Chem. Rev. **77**, 815 (2008).
[29]D. Mazzier, M. Mba, M. Zerbetto, and A. Moretto, Chem. Commun. **50**, 4571 (2014).
[30]H. Kim, D. Bedrov, G. D. Smith, S. Shenogin, and P. Keblinski, Phys. Rev. B **72**, 085454 (2005).
[31]G. Angelini, C. Cusan, P. De Maria, A. Fontana, M. Maggini, M. Pierini, M. Prato, S. Schergna, and C. Villani, Eur. J. Org. Chem. **2005**, 1884 (2005).
[32]E. Y. Zhang, and C. R. Wang, Curr. Opin. Colloid Int. Sci. **14**, 148 (2009).
[33]V. K. Periya, I. Koike, Y. Kitamura, S. I. Iwamatsu, and S. Murata, Tetrahedron Lett. **45**, 8311 (2004).
[34]G. Angelini, P. De Maria, A. Fontana, M. Pierini, M. Maggini, F. Gasparrini, and G. Zappia, Langmuir **17**, 6404 (2001).
[35]D. M. Guldi, M. Maggini, S. Mondini, F. Guerin, and J. H. Fendler, Langmuir **16**, 1311 (2000).
[36]M. Li, S. Ishihara, Q. Ji, M. Akada, J. P. Hill, and K. Ariga, Sci. Technol. Adv. Mater. **13**, 053001 (2012).
[37]N. Nakashima, T. Ishii, M. Shirakusa, T. Nakanishi, H. Murakami, and T. Sagara, Chem. - Eur. J. **7**, 1766 (2001).
[38]J. N. Israelachvili, D. J. Mitchell, and B. W. Ninham, J. Chem. Soc. Faraday Trans. II **72**, 1525 (1976).
[39]J. N. Israelachvili, *Intermolecular and Surface Forces*, 3rd ed. (Academic Press, 2011).
[40]T. Nakanishi, Y. Shen, J. Wang, H. Li, P. Fernandes, K. Yoshida, S. Yagai, M. Takeiuchi, K. Ariga, D. G. Kurth, and H. Möhwald, J. Mater. Chem. **20**, 1253 (2010).
[41]J. N. Tisserant, R. Hany, E. Wimmer, A. Sánchez-Ferrer, J. Adamcik, G. Wicht, F. Nüesch, D. Rentsch, A. Borgschulte, R. Mezzenga, and J. Heier, Macromolecules **47**, 721 (2014).
[42]Y. Zhao and G. Chen, Struct. Bonding **159**, 23 (2014).
[43]P. Brough, D. Bonifazi, and M. Prato, Tetrahedron **62**, 2110 (2006).
[44]S. M. Mortuza and S. Banerjee, J. Chem. Phys. **137**, 244308 (2012).
[45]K. S. Kumar and A. Patnaik, Langmuir **27**, 11017 (2011).
[46]R. A. Guirado-López and M. E. Rincón, J. Chem. Phys. **125**, 154312 (2006).
[47]A. Piątek, A. Dawid, and Z. Gburski, Spectrochim. Acta, Part A **79**, 819 (2011).
[48]S. S. Gayathri and A. Patnaik, J. Chem. Phys. **124**, 131104 (2006).
[49]S. S. Gayathri, A. K. Agarwal, K. A. Suresh, and A. Patnaik, Langmuir **21**, 12139 (2005).
[50]S. S. Gayathri and A. Patnaik, Langmuir **23**, 4800 (2007).
[51]V. Georgakilas, F. Pellarini, M. Prato, D. M. Guldi, M. Melle-Franco, and F. Zerbetto, Proc. Natl. Acad. Sci. U.S.A. **99**, 5075 (2002).
[52]M. Prato and M. Maggini, Acc. Chem. Res. **31**, 519 (1998).
[53]The PyMOL Molecular Graphics System, Version 1.2r3pre, Schrödinger, LLC.
[54]M. J. Frisch, G. W. Trucks, H. B. Schlegel, G. E. Scuseria, M. A. Robb, J. R. Cheeseman, G. Scalmani, V. Barone, B. Mennucci, G. A. Petersson, H. Nakatsuji, M. Caricato, X. Li, H. P. Hratchian, A. F. Izmaylov, J. Bloino, G. Zheng, J. L. Sonnenberg, M. Hada, M. Ehara, K. Toyota, R. Fukuda, J. Hasegawa, M. Ishida, T. Nakajima, Y. Honda, O. Kitao, H. Nakai, T. Vreven, J. A. Montgomery, Jr., J. E. Peralta, F. Ogliaro, M. Bearpark, J. J. Heyd, E. Brothers, K. N. Kudin, V. N. Staroverov, R. Kobayashi, J. Normand, K. Raghavachari, A. Rendell, J. C. Burant, S. S. Iyengar, J. Tomasi, M. Cossi, N. Rega, J. M. Millam, M. Klene, J. E. Knox, J. B. Cross, V. Bakken, C. Adamo, J. Jaramillo, R. Gomperts, R. E. Stratmann, O. Yazyev, A. J. Austin, R. Cammi, C. Pomelli, J. W. Ochterski, R. L. Martin, K. Morokuma, V. G. Zakrzewski, G. A. Voth, P. Salvador, J. J. Dannenberg, S. Dapprich, A. D. Daniels, Ö. Farkas, J. B. Foresman, J. V. Ortiz, J. Cioslowski, and D. J. Fox, Gaussian 09, Revision A.01, Gaussian, Inc., Wallingford CT, 2009.
[55]H. Sun, Macromolecules **28**, 701 (1995).
[56]L. A. Girifalco, J. Phys. Chem. **95**, 5370 (1991).
[57]L. Monticelli, J. Chem. Theory Comput. **8**, 1370 (2012).
[58]W. L. Jorgensen and J. Gao, J. Phys. Chem. **90**, 2174 (1986).
[59]D. J. Price and C. L. Brooks, J. Chem. Phys. **33**, 2363 (2004).
[60]L. Martínez, R. Andrade, E. G. Birgin, and J. M. Marítnez, J. Comput. Chem. **30**, 2157 (2009).
[61]S. J. Plimpton, J. Comput. Phys. **117**, 1 (1995).
[62]S. R. Varanasi, O. A. Guskova, and J.-U. Sommer, "Water around fullerene dyads: A molecular dynamics simulation study," J. Chem. Phys. (unpublished).
[63]C. Balzarek and D. R. Tyler, Angew. Chem., Int. Ed. **38**, 2406 (1999).
[64]M. Sano, K. Oishi, T. Ishi-I, and S. Shinkai, Langmuir **16**, 3773 (2000).
[65]S. Tsonchev, G. C. Schatz, and M. A. Ratner, Nano Lett. **3**, 623 (2003).
[66]G. Fernández, E. M. Pérez, L. Sánchez, and N. Martín, J. Am. Chem. Soc. **130**, 2410 (2008).
[67]I. M. Mahmud, N. Zhou, L. Wang, and Y. Zhao, Tetrahedron **64**, 11420 (2008).
[68]H. Kato, C. Böttcher, and A. Hirsch, Eur. J. Org. Chem. **2007**, 2659 (2007).
[69]S. Zhou, C. Burger, B. Chu, M. Sawamura, N. Nagahama, M. Toganoh, U. E. Hackler, H. Isobe, and E. Nakamura, Science **291**, 1944 (2001).
[70]Yu. A. Shchipunov and E. V. Shumilina, J. Colloid Int. Sci. **161**, 125 (1993).
[71]A. E. Stearn and H. Eyring, Chem. Rev. **29**, 509 (1941).
[72]R. B. Corey and L. Pauling, Rev. Sci. Instrum. **24**, 621 (1953).
[73]B. Lee and F. M. Richards, J. Mol. Biol. **55**, 379 (1971).
[74]R. F. W. Bader, M. T. Carroll, J. R. Cheeseman, and C. Chang, J. Am. Chem. Soc. **109**, 7968 (1987).
[75]D. X. Zhao and Z. Z. Yang, J. Theor. Comput. Chem. **07**, 303 (2008).
[76]H. Kim, D. Bedrov, and G. D. Smith, J. Chem. Theory Comput. **4**, 335 (2008).
[77]S. Banerjee, J. Chem. Phys. **138**, 044318 (2013).
[78]C. Tanford, *The Hydrophobic Effect* (Wiley, New York, 1973).
[79]R. Nagarajan, in *Surfactant Science and Technology: Retrospects and Prospects* (CRC Press, 2014).
[80]A. V. Dobrynin, M. Rubinstein, and S. P. Obukhov, Macromolecules **29**, 2974 (1996).
[81]J. M. Y. Carillo and A. V. Dobrynin, Langmuir **25**, 13158 (2009).
[82]M. N. Tamashiro and H. Schiessel, Phys. Rev. E **74**, 021412 (2006).
[83]W. Humphrey, A. Danke, and K. Schulten, J. Mol. Graph. **14**, 33 (1996).
[84]See supplementary material at http://dx.doi.org/10.1063/1.4896559 for Figures 1 and 2.
[85]D. N. Theodoru and U. W. Suter, Macromolecules **18**, 1467 (1985).
[86]S. Ber, R. R. M. Jones, and J. S. Johnson, Jr., J. Phys. Chem. **96**, 5611 (1992).
[87]F. Hofmeister, Arch. Exp. Pathol. Pharmakol. **24**, 247 (1888).
[88]Y. Marcus, Chem. Rev. **109**, 1346 (2009).
[89]E. A. Algaer and N. F. A. van der Vegt, J. Phys. Chem. B **115**, 13781 (2011).
[90]N. Schwierz, D. Horinek, and R. R. Netz, Langmuir **29**, 2602 (2013).
[91]P. Jungwirth and P. S. Cremer, Nat. Chem. **6**, 261 (2014).
[92]D. Cui, S. Ou, E. R. Peters, and S. Patel, J. Phys. Chem. B **118**, 4490 (2014).
[93]B. A. Moyer and P. V. Bonnesen, "Physical factors in anion separation," in *Supramolecular Chemistry of Anions*, edited by A. Bianchi, K. Bowman-James, and E. Garcia-Espana (Wiley-VCH Inc., New York, 1979), pp. 1–44.
[94]C. Calero, J. Faraudo, and D. Bastos-Gonzáles, J. Am. Chem. Soc. **133**, 15025 (2011).
[95]V. Subramanian and W. A. Ducker, Langmuir **16**, 4447 (2000).
[96]D. M. Guldi, Res. Chem. Intermed. **23**, 653 (1997).